

Electronic Supplementary Information for "Effect of encapsulated protein on the dynamics of lipid sponge phase: A neutron spin echo and molecular dynamics simulation study"

Jennifer Gilbert,^{a,b} Inna Ermilova,^c Michihiro Nagao,^{d,e,f} Jan Swenson,^c and Tommy Nylander^{a,b,g,*}

^a Division of Physical Chemistry, Department of Chemistry, Naturvetarvägen 14, Lund University, 22362 Lund, Sweden.

^b NanoLund, Lund University, Professorsgatan 1, 223 63 Lund, Sweden.

^c Department of Physics, Chalmers University of Technology, 412 96 Gothenburg, Sweden.

^d NIST Center for Neutron Research, National Institute of Standards and Technology, Gaithersburg, Maryland 20899, USA.

^e Department of Materials Science and Engineering, University of Maryland, College Park, Maryland 20742, USA.

^f Department of Physics and Astronomy, University of Delaware, Newark, Delaware 19716, USA.

^g Lund Institute of Advanced Neutron and X-Ray Science, Scheelevägen 19, 223 70 Lund, Sweden.

* Corresponding author: tommy.nylander@fkem1.lu.se

Structures of the Cubic and Sponge Phase

In this work, the dynamics of lipid sponge phase nanoparticles with and without encapsulated enzymes are discussed and related to their structure. The inverse bicontinuous cubic phase with Pn3m (double diamond) space group is a highly ordered structure, with a well defined unit cell, water channel size and angle at which the water channels meet. As described in the main manuscript, sponge phase can be considered a 'melted' cubic phase. By showing the equivalent view of each unit cell, the figure below aims to highlight the similarities between the structures, such as the water channel network, but also their differences, including the sponge phase's disorder, lack of a well defined unit cell and swollen channel size. It should be noted that this is only a representation of the sponge phase unit cell; due to its disordered nature, there are many possible unit cell structures.

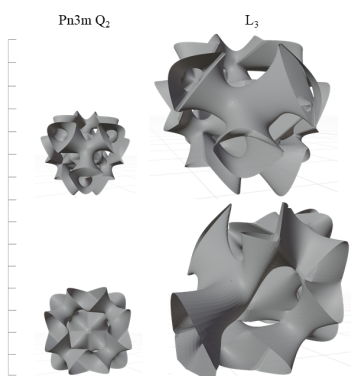


Figure S1 Schematic structures of the inverse bicontinuous cubic phase (Pn3m) and sponge phase. The grey surface represents the interface between the inner and outer leaflets of the bilayer. Bottom line: Unit cell. Top: Another view to highlight tetrahedral geometry of water channel.

Cryo-TEM images of L₃NPs

The structure and morphology of the L₃NPs containing β -galactosidase and aspartic protease were imaged using cryo-transmission electron microscopy, as described previously¹.

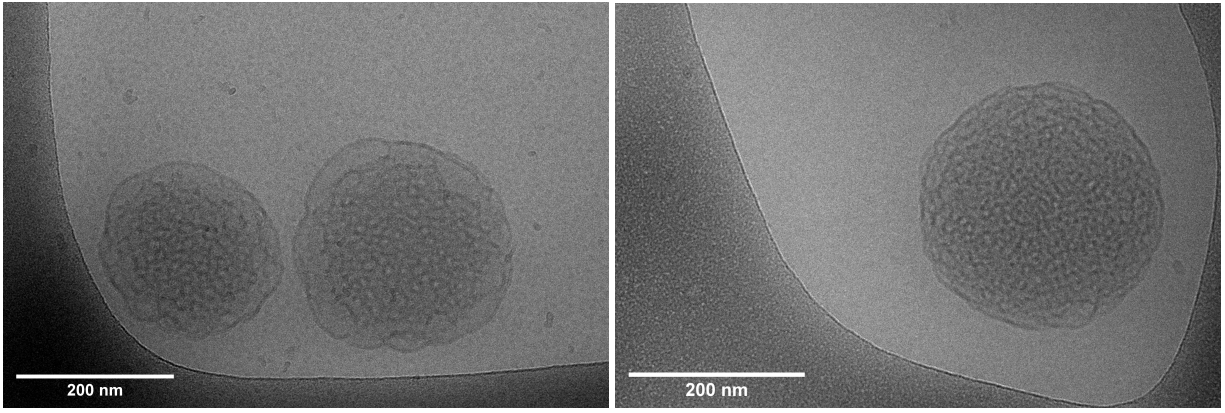


Figure S2 Cryo-TEM images of (left) L₃NPs containing aspartic protease and (right) L₃NPs containing β -galactosidase.

NSE Experimental Set Up

All samples were measured at 25 °C in custom made sample holders with a sample thickness of 1 mm. D₂O was measured as the sample background and charcoal and carbon powder as a standard for instrument resolution. The neutron scattering intensity was measured at 4 nominal q values: 0.045 Å⁻¹ and 0.06 Å⁻¹ using a neutron wavelength, $\lambda = 11$ Å and 0.09 Å⁻¹ and 0.12 Å⁻¹ using $\lambda = 8$ Å on a two-dimensional area detector. The detector was then divided into 5 areas so that we took multiple q values from each nominal q value, and areas with insufficient intensity were discarded.

Derivation of Expanded Zilman and Granek Model

The intermediate scattering functions (ISFs) were fit according to a modified Zilman and Granek model to determine the bending rigidity of the bilayer. The original model proposed by Zilman and Granek considers the membrane as an ensemble of single non-interacting membrane plaquettes of size $L \times L$, which are randomly oriented and described by the Helfrich bending free energy^{2,3}. The relaxation function of the structure factor due to thermal undulations was shown to be:

$$S(q, t) = \exp(-(\Gamma t)^{\frac{2}{3}}) \quad (1)$$

where t is Fourier time (ns) and Γ is relaxation rate (ns⁻¹). This relaxation function was expanded by Hoffmann to include the contribution of diffusion as follows⁴:

$$S(q, t) = \exp(-Dq^2 t) \exp(-(\Gamma t)^{\frac{2}{3}}) \quad (2)$$

where D is diffusion constant (as determined by dynamic light scattering) and q is scattering vector. This expression for $S(q, t)$ was used to fit the ISFs, therefore determine Γ , using values of D calculated from DLS measurements included in other work on the same system^{5,6}. In the q range where the Zilman and Granek model is valid, the relaxation rate Γ is equal to the relaxation rate for bending fluctuations Γ_b , is given by the expression:

$$\Gamma_b = 0.025\gamma \sqrt{\frac{k_b T}{\bar{\kappa}}} \frac{k_b T}{\eta} q^3 \quad (3)$$

where $\bar{\kappa}$ is the effective bilayer bending modulus, η is solvent viscosity and γ accounts for orientational averaging for an isotropic ensemble of plaquettes, which is suitable to describe the sponge phase. When $\bar{\kappa} \gg k_b T$, γ goes to 1, which is assumed here.

In the original Zilman and Granek model, the bilayer is treated as a single thin elastic sheet, such that the two leaflet nature of the bilayer is ignored and all dissipation in the bilayer is due to viscous losses in the solvent³. Over the length and time scales of NSE, it is important to account for the two-leaflet nature of the bilayer. Bending such a bilayer creates density difference between the inner and outer leaflets that cannot be relaxed instantaneously at the NSE length and time scales, which can be suitably accounted for using the effective bending modulus^{7,8}:

$$\bar{\kappa} = \kappa + 2h^2 k_m \quad (4)$$

where κ is the intrinsic bilayer bending modulus, h is the height of the neutral surface from the bilayer midplane and k_m is the monolayer area compressibility modulus. k_m can be expressed in terms of h_c , the monolayer (hydrocarbon) thickness, and κ_m , the monolayer bending modulus, such that⁹:

$$k_m = \frac{12\kappa_m}{h_c^2} \quad (5)$$

Using the relation between the monolayer and bilayer bending moduli:

$$\kappa_m = \frac{\kappa}{2} \quad (6)$$

After substitution of the latter equations into the former, the effective bending modulus can be re-expressed in terms of the ratio between the height of the neutral surface from the bilayer midplane and the monolayer (hydrocarbon) thickness:

$$\bar{\kappa} = (1 + 48(\frac{h}{2h_c})^2)\kappa \quad (7)$$

The value of $h/2h_c$ is widely debated, with various values given in literature, but, as per previous work in NSE fitting, here we use the value 0.5¹⁰. Upon modification with these expressions, the original expression for the relaxation rate can be rewritten as:

$$\Gamma_b = 0.0069 \sqrt{\frac{k_b T}{\kappa} \frac{k_b T}{\eta}} q^3 \quad (8)$$

The above expression for Γ_b was used to calculate bending rigidity. It is noted here, however, that the absolute values of the bending modulus calculated using NSE is an ongoing discussion⁴, while there is in general consensus that relative trends estimated through an NSE experiment are correct. The relative values were, therefore, calculated and discussed here as follows:

$$\kappa_{rel} = \frac{\kappa}{\kappa_{empty}} \quad (9)$$

where κ_{rel} is the bending modulus normalised to κ_{empty} , the bending modulus for the empty L₃NPs.

Fitting of Intermediate Scattering Functions

After the initial data reduction, the point corresponding to $q = 0.0583 \text{ \AA}^{-1}$ was excluded from all analyses due to large instrumental error. All measured ISFs were fit using equation (2), as shown below in Figure S2 plotted as solid black lines.

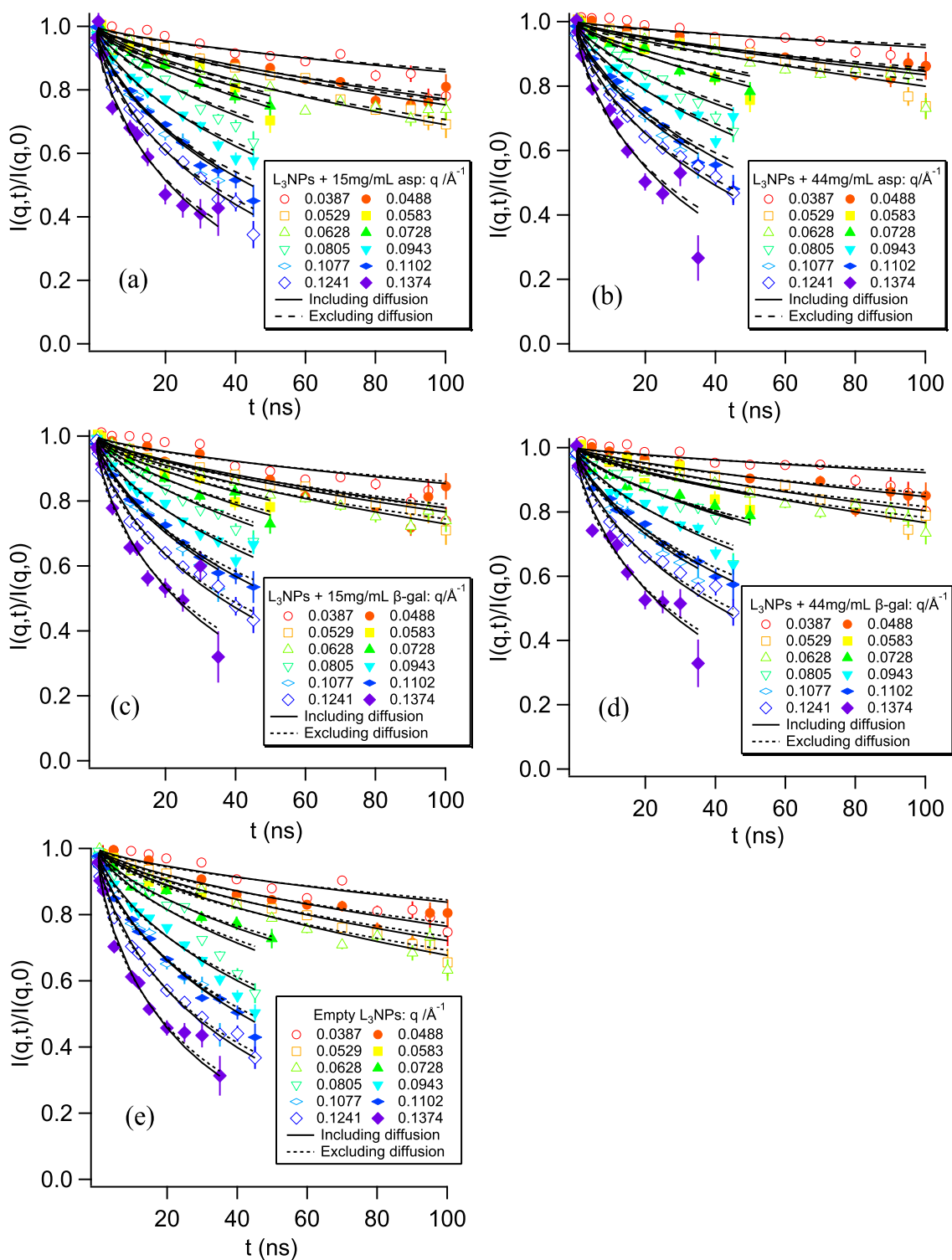


Figure S3 ISFs for L₃NPs with (a) 15mg/mL aspartic protease, (b) 44mg/mL aspartic protease, (c) 15mg/mL β -galactosidase, (d) 44mg/mL β -galactosidase and (e) without enzyme. Fits including diffusion (equation (2)) are plotted as solid black lines and fits excluding diffusion (equation (1)) are plotted as dashed black lines.

Fitting of Γ/q^3 vs q Plots

Membrane bending rigidity κ was determined by fitting the data in the plots of Γ/q^3 against q within the Zilman and Granek regime ($0.7 \text{ \AA}^{-1} \leq q \leq 0.13 \text{ \AA}^{-1}$) described in the preceding section, with equation 8 (Figure S3). An exception was made in the case of L_3 NPs + 44 mg/mL aspartic protease, in which the data for $0.08 \text{ \AA}^{-1} \leq q \leq 0.13 \text{ \AA}^{-1}$ was fit, as the excluded point largely deviated from the constant Γ/q^3 value, most likely because of the influence of the static structure factor peak near this q value due to the proximity of this aspartic protease concentration to the cubic phase transition boundary. It should be noted that, when the q range for the other samples was also restricted to this range, the calculated κ values were the same within the error.

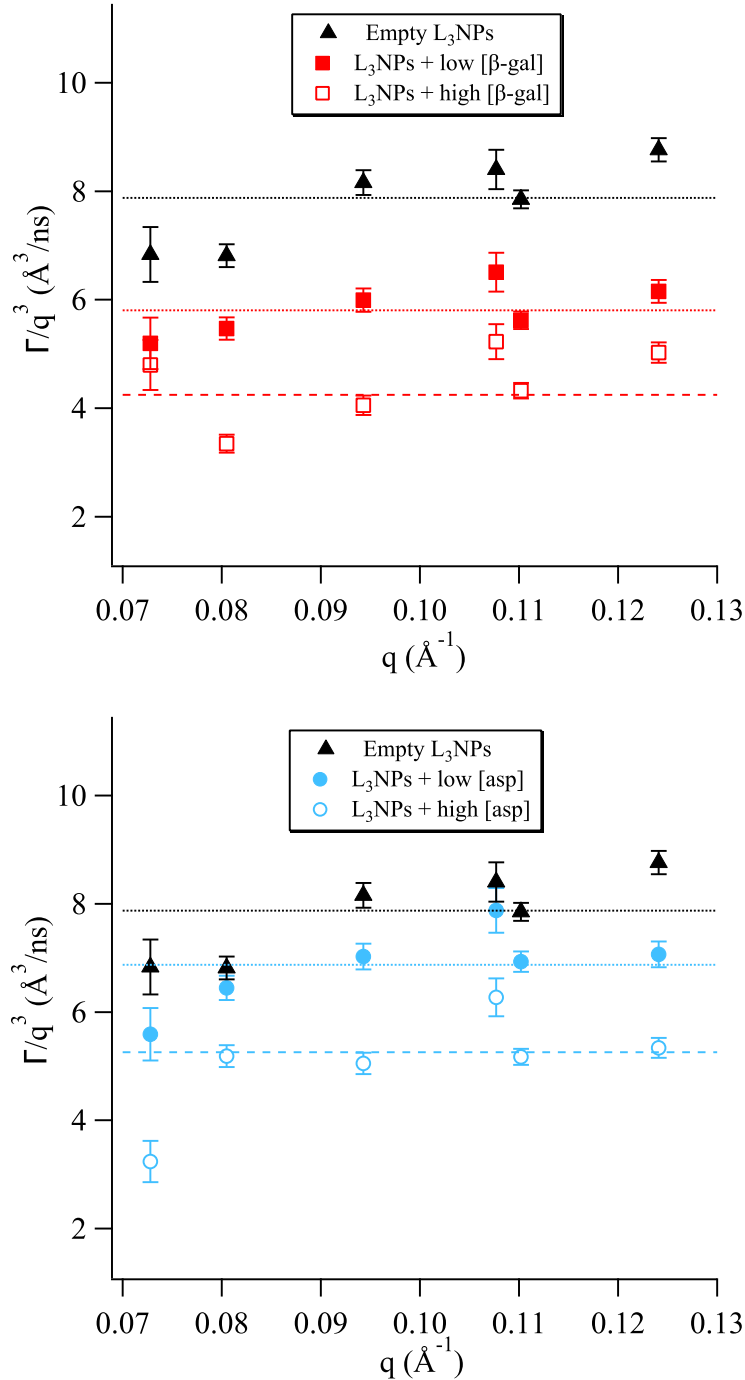


Figure S4 The normalised relaxation rate Γ/q^3 vs q was plotted for sponge phase nanoparticles with different concentrations of encapsulated enzymes in the q range where the model is valid. The horizontal lines show the fit of the Zilman and Granek model for the relaxation rate Γ/q^3 for bending fluctuations (equation 2).

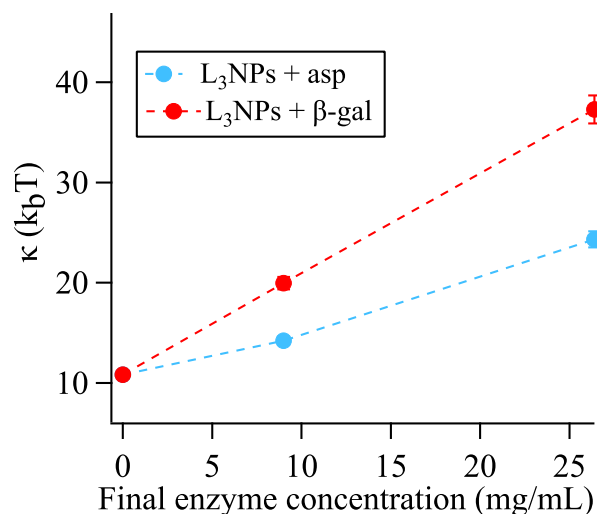
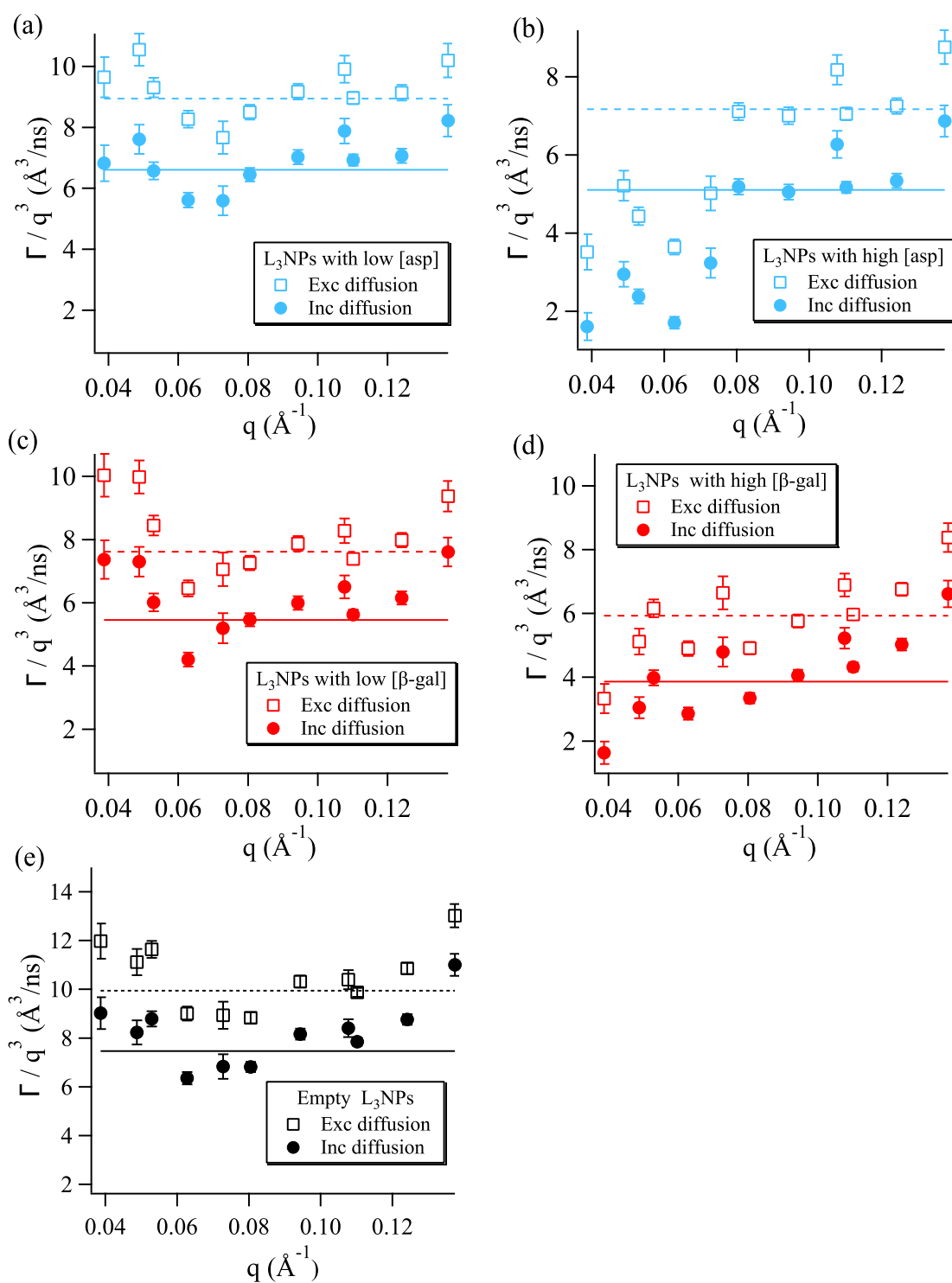


Figure S5 The non-normalised membrane bending moduli κ , extracted from the linear fits of equation 2 shown in Figure 1, are shown plotted against the final enzyme concentration in the sponge phase nanoparticles. Dotted lines included only to indicate trend.

Effect of Excluding Diffusion

For comparison, the ISFs were also fitted with equation (1), which assumes the diffusion is slow enough to be $\exp(-Dq^2t) = 1$. As can be seen in Figure S2, where this alternative fit was plotted as dashed black lines, there are only minor differences between the fits, mostly in the shape of the curves, and both fits resulted in similar chi-squared values for all samples.

The resulting Γ values were also fit as described in the previous section, shown in Figure S5, in order to determine the bending rigidity, when diffusion is excluded. As expected, the Γ values are higher when diffusion is excluded, due to the increased contribution of the Zilman and Granek term, resulting in slightly lower calculated bending rigidities.



[H]

Figure S6 Comparison between fits for the bending rigidity including and excluding the contribution from diffusion for L₃NPs with (a) 15mg/mL aspartic protease, (b) 44mg/mL aspartic protease, (c) 15mg/mL β -galactosidase, (d) 44mg/mL β -galactosidase and (e) without enzyme. Fits including diffusion are plotted as solid black lines and fits excluding diffusion are plotted as dashed black lines.

Parametrization of Model Lipids

The general equation for the SLipids FF can be written as follows:

$$E_{ff} = E_{bonded} + E_{non-bonded} \quad (10)$$

where E_{bonded} stands for potentials describing bonded interactions, such as angle bending, bond stretching, Urey-Bradley bond-angle vibration and dihedral rotation and $E_{non-bonded}$ is the potential determining the non-bonded interactions, such as sum of van der Waals (Lennard-Jones potential) and electrostatic (Coulombic potential) interactions. The latter potentials can be described by equation (10):

$$E_{Coulomb} = \sum_{i,j \neq i} \frac{q_i q_j}{4\pi\epsilon_0 r_{ij}} \quad (11)$$

where q_i and q_j are the partial atomic charges of non-bonded atoms i and j respectively, r_{ij} is the distance between those atoms and ϵ_0 is the vacuum permittivity. In this work, the parameters for Coulombic potential were derived for lipid tails using the same philosophy of calculations as in earlier versions of SLipids FF¹¹.

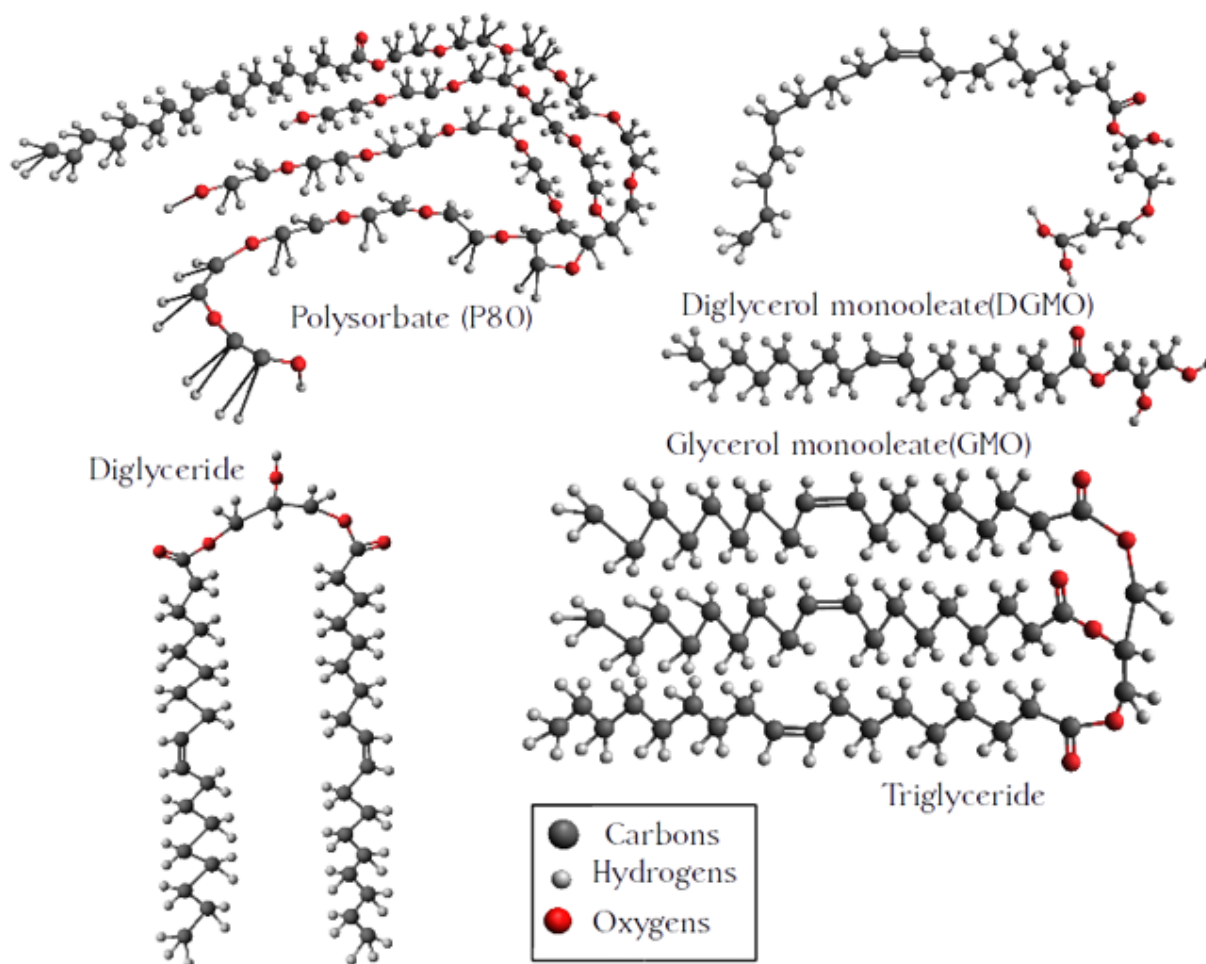


Figure S7 Structures of lipids used in molecular dynamics simulations. The models are available for download from the Zenodo repository.

Secondary Structure Evolution of Encapsulated Aspartic Protease

Figure S7 demonstrates the evolution of the secondary structure of aspartic protease during the last 100 ns of the simulation. Here a certain color denotes a particular secondary structure. Most of the amino acid residues do not change their secondary structure during the time of the calculation, which can be seen as the same color on the figure. Although some small changes can be detected from the figure, such as minor fluctuations from “Coil” to “Turn”, or changes from “Turn”/“Coil” to “Extended conformation”, these are not considerable. Such a stability of the secondary structure shows that the chosen group of lipids are good candidates as preservatives for proteins.

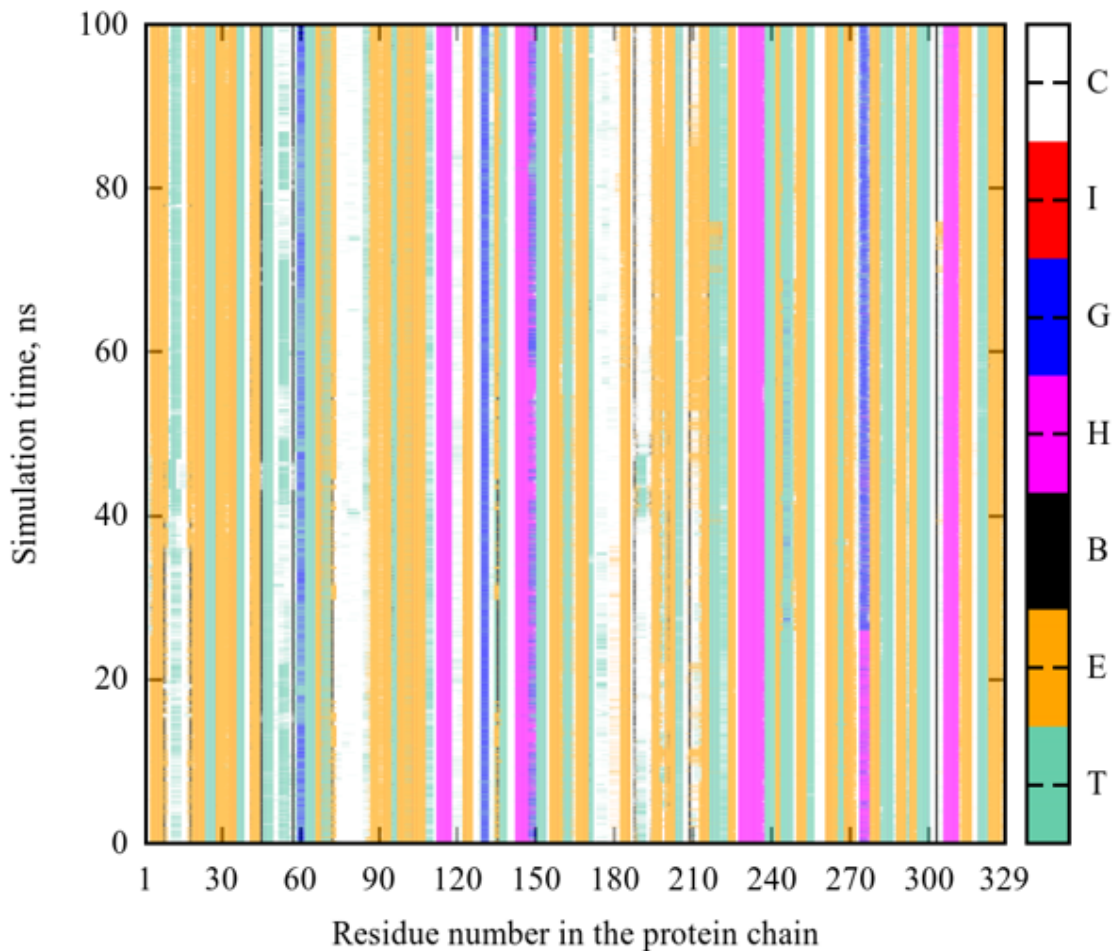


Figure S8 Secondary structure of aspartic protease during the last 100 ns of simulation. Codes for the secondary structures are the following: “T” - turn, “E” - extended conformation, “B” - isolated β -bridge, “H” - α -helix, “G” - 3_{10} -helix, “I” - π -helix. The structures are named using VMD software^{12,13}.

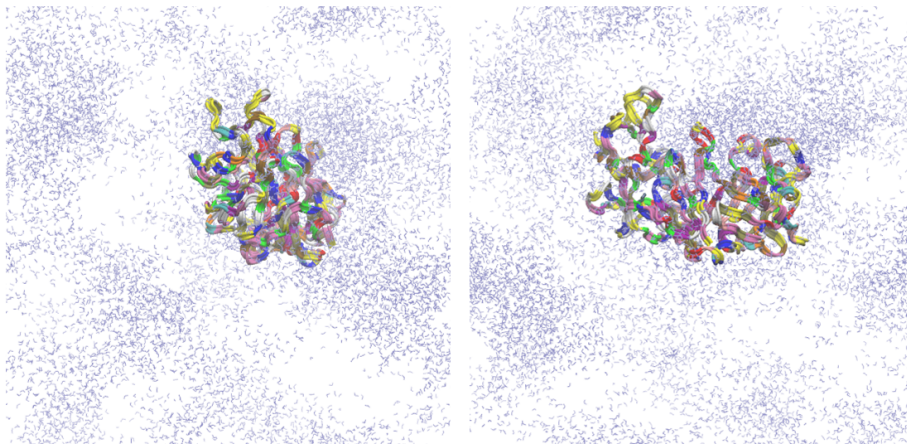


Figure S10 Snapshots from simulation containing aspartic protease, with the water molecules shown in blue. For clarity and to highlight the protein's position relative to the water channels, the lipids are not shown but reside in the space not occupied by the water molecules.

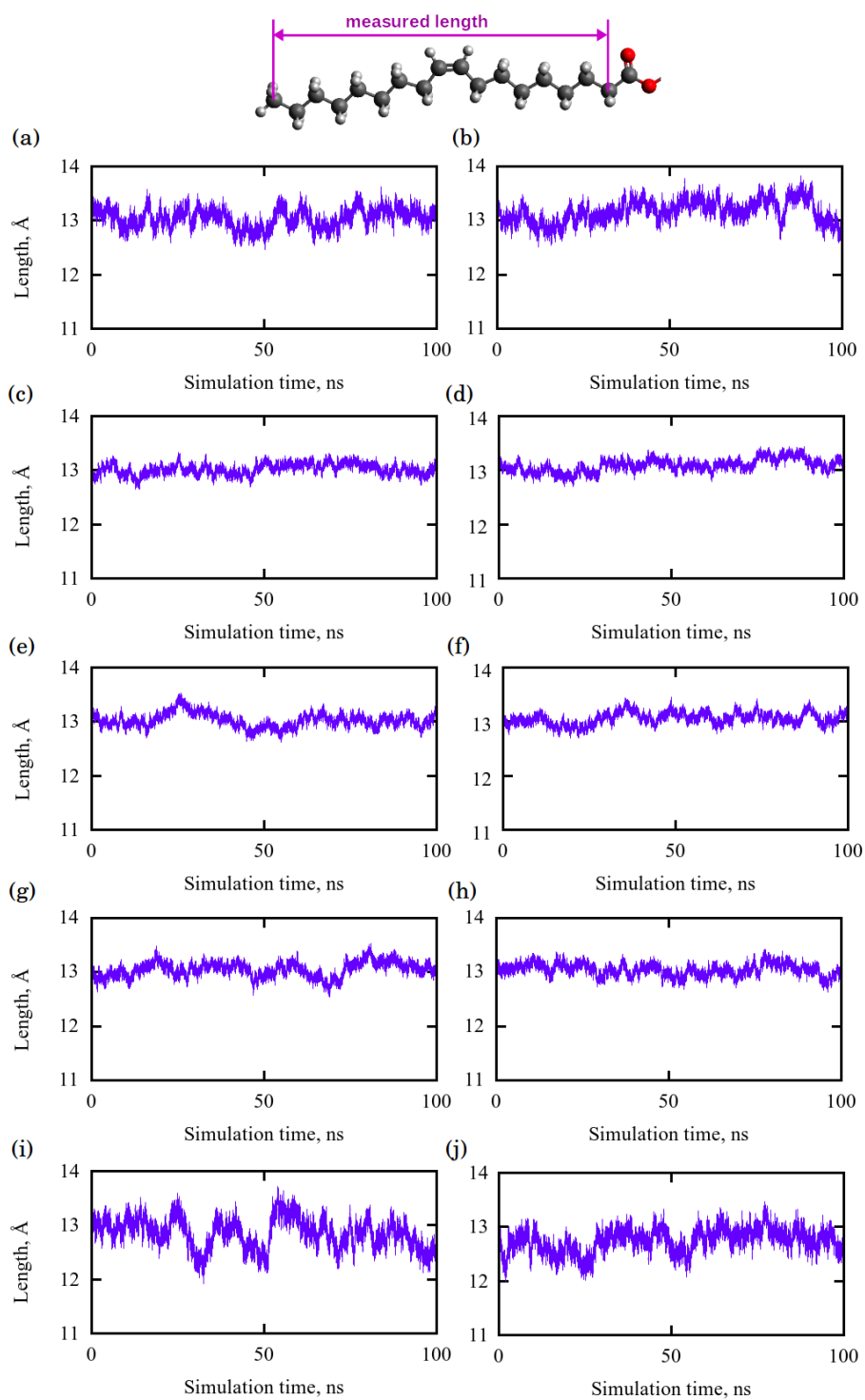


Figure S11 Fluctuation of the lipid tail length over the last 100ns of the simulation. LHS: no protein, RHS: with protein. (a,b) P80, (c,d) DGMO, (e,f) GMO-50, (g,h) diglycerides, (i,j) triglycerides. These calculated values agree very well with fitted reflectometry values for the same lipid system¹⁴.

Table 1 Number of hydrogen bonds in simulated systems during last 100 ns. The number of hydrogen bonds between protein and water was 418. The number of hydrogen bonds between lipid head-groups was 1220 for both simulated systems. The number of lipids and lipid composition was the same in both simulations.

Lipid	Number of lipid-H ₂ O H-bonds (no protein)	Number of lipid-H ₂ O H-bonds (protein)	Number of lipid-protein H-bonds
P80	2920	2835	16
DGMO	1372	1387	8
GMO	1045	1048	12
Diglycerides	367	363	1
Triglycerides	49	44	0

Notes and references

- [1] M. Valldeperas, A. P. Dabkowska, G. K. Pálsson, S. Rogers, N. Mahmoudi, A. Carnerup, J. Barauskas and T. Nylander, *Soft Matter*, 2019, **15**, 2178–2189.
- [2] W. Helfrich, *Zeitschrift fur Naturforschung. Teil C: Biochemie, Biophysik, Biologie, Virologie*, 1973, **28**, 693–703.
- [3] A. G. Zilman and R. Granek, *Physical Review Letters*, 1996, **77**, 4788–4791.
- [4] I. Hoffmann, *Frontiers in Physics*, 2021, **8**, 602.
- [5] J. Gilbert, M. Valldeperas, S. K. Dhayal, J. Barauskas, C. Dicko and T. Nylander, *Nanoscale*, 2019, **11**, 21291–21301.
- [6] M. Valldeperas, M. Talaikis, S. K. Dhayal, M. Velička, J. Barauskas, G. Niaura and T. Nylander, *Biophysical Journal*, 2019, **117**, 829–843.
- [7] U. Seifert and S. A. Langer, *Europhysics Letters (EPL)*, 1993, **23**, 71–76.
- [8] M. C. Watson and F. L. H. Brown, *Biophysical Journal*, 2010, **98**, L9–L11.
- [9] D. Boal, *Mechanics of the Cell*, Cambridge University Press, Cambridge, 2nd edn, 2012.
- [10] M. Nagao, E. G. Kelley, R. Ashkar, R. Bradbury and P. D. Butler, *The Journal of Physical Chemistry Letters*, 2017, **8**, 4679–4684.
- [11] I. Ermilova and A. P. Lyubartsev, *The Journal of Physical Chemistry B*, 2016, **120**, 12826–12842.
- [12] W. Humphrey, A. Dalke and K. Schulten, *Journal of Molecular Graphics*, 1996, **14**, 33–38.
- [13] M. Yahyavi, S. Falsafi-Zadeh, Z. Karimi, G. Kalatarian and H. Galehdari, *Bioinformation*, 2014, **10**, 548–550.
- [14] M. Valldeperas Badell, *PhD thesis*, Lund University, 2019.